Available online at www.sciencedirect.com
SCIENCE DIRECT®
Journal of Catalysis 220 (2003) 457–467
JOURNAL OF CATALYSIS
www.elsevier.com/locate/jcat

Effects of preparation method and sulfur poisoning on the hydrogenation and ring opening of tetralin on NiW/zirconium-doped mesoporous silica catalysts

D. Eliche-Quesada,[a] J. Mérida-Robles,[a] P. Maireles-Torres,[a] E. Rodríguez-Castellón,[a] G. Busca,[b] E. Finocchio,[b] and A. Jiménez-López [a,*]

[a] *Departamento de Química Inorgánica, Cristalografía y Mineralogía (Unidad Asociada del Instituto de Catálisis y Petroleoquímica, CSIC), Facultad de Ciencias, Universidad de Málaga, 29071 Málaga, Spain*

[b] *Department of Chemical and Process Engineering, University of Genova, I-16129 Genova, Italy*

Received 4 April 2003; revised 2 June 2003; accepted 3 June 2003

Abstract

Nickel-tungsten supported on zirconium-doped mesoporous silica catalysts was prepared by using different methodologies and successfully tested at the hydrogenation and ring opening of tetralin. The preparation method has an important influence on surface properties such as dispersion, location, and reducibility of NiW species as deduced from H_2-TPR, H_2 chemisorption, FTIR spectra of CO adsorbed, and XPS studies. Thus, when nickel, in the form of nickel citrate, is first incorporated followed by tungsten, a catalyst is obtained with the highest acidity and the best catalytic performance, yielding a full conversion of tetralin (100%) as well as high yields of hydrogenation (42.7%) and ring-opening (56.1%) products under mild conditions (6.0 MPa of H_2 and 375 °C). This catalyst exhibits a good thiotolerance in the presence of 300 ppm of dibenzothiophene in the feed, maintaining a high catalytic activity in the hydrogenation and ring-opening reactions after 6 h on stream.

Keywords: Bimetallic nickel–tungsten catalysts; MCM-41; Tetralin hydrogenation; Ring opening

1. Introduction

The current demand for high-quality diesel fuels is growing quickly, and will continue to grow for the foreseeable future. Simultaneously, environmental regulations are becoming more stringent. New diesel fuel specifications will mainly require a reduction of sulfur and aromatic content, while the cetane number will be set to a minimum value of about 53 units. Aromatics, especially polycyclics, usually have very low cetane numbers, while *n*-paraffin hydrocarbons have relatively high ones. Thus, a key factor for improving the cetane number is to decrease the aromatic content, especially polyaromatics, in distillates; while avoiding excessive cracking to obtain high yields of upgraded diesel fuels.

Catalytic hydrogenation is an important process for reducing the aromatic content in liquid fuels or solvents [1], because, after a desulfurization and denitrogenation treatment, they usually still contain a relatively high percentage of aromatics, which not only generate undesired emissions of particles in exhaust gases but also decrease the cetane number. The restrictions for exhaust emissions can be met by deep hydrotreating, which typically consists of a two-stage process with a conventional hydrotreating catalyst (CoMo, NiMo, NiW) at the first stage and a more active hydrogenation catalyst (Ni, Pt) at the second stage, as reviewed by Cooper and Donnis [2]. The cetane number can be ameliorated by the hydrogenation and ring opening of aromatics, and so new catalytic systems and hydrotreating processes must be developed in order to minimize the emissions and improve the fuel quality. Thus, many research efforts are being devoted to the synthesis of more active hydrotreating catalysts by the addition of a second promotor such as phosphorus or boron [3,4] or by using different supports [5,6]. In this sense, in recent years, there has been an explosive

* Corresponding author.
E-mail address: ajimenezl@uma.es (A. Jiménez-López).

0021-9517/$ – see front matter
doi:10.1016/S0021-9517(03)00271-9

growth in the synthesis of new mesoporous materials with a controlled and variable pore-size distribution, composition, and texture. Some of these new materials have already shown very interesting applications in hydrodesulfurization, hydrodenitrogenation, and hydrocracking reactions [6,7].

On the other hand, we have recently reported that the catalytic performance of catalysts greatly depends on the preparation procedure. Thus, the use of nickel citrate, instead of nickel nitrate, as a nickel source for the preparation of nickel supported on zirconium-doped mesoporous silica, with high nickel loading (ca. 20 wt%), allows highly active catalysts in the hydrogenation and ring opening of tetralin to be obtained [8].

The goal of the present work is to evaluate the influence of the preparation of NiW catalysts supported on zirconium-doped mesoporous silica on their catalytic performance in the hydrogenation and ring opening of tetralin. Moreover, the Ni/W ratio, the reaction temperature, the contact time, and the H_2/tetralin molar ratio have been optimized in order to increase the production of cracking compounds with improved cetane numbers. Further, the thiotolerance of these catalysts has also been evaluated by introducing dibenzothiophene in the feed. The more acidic zirconium-doped mesoporous silica was chosen as a support for inorganic phases with catalytic activity instead of a pure mesoporous silica support since better results are obtained [8].

Hydrogenation of naphthalene has been widely used as a model reaction for evaluating the hydrogenation properties [9]. However, the hydrogenation of monoaromatics (deep hydrogenation) is more difficult than that of polyaromatics [10], so we have chosen tetralin as the model molecule to test the catalytic performance of these new catalysts for the deep hydrogenation of aromatics.

2. Experimental

2.1. Catalyst preparation

The supported NiW catalysts were prepared by incipient wetness impregnation of a powdered zirconium-doped mesoporous silica (Si/Zr molar ratio of 5, SiZr5), which was synthesized following the method described elsewhere [11], but with a reduced reaction time at room temperature from 4 days to only 1.

In order to evaluate the influence of the impregnation sequence on the catalytic properties, different preparation procedures were studied. Two series of catalysts were synthesized by consecutive impregnation with ammonium tungstate and nickel citrate aqueous solutions. This latter solution was prepared by mixing nickel carbonate and citric acid in a 3:2 molar ratio in deionized water and heating until the suspension turned a bright green color. After each impregnation step, the samples were dried at 60 °C. The materials were then calcined at 550 °C for 4 h and labeled as NiW(x) or W(x)Ni, depending on the impregnation sequence, where the order reflected the addition of metal precursors. The nickel loading, 20 wt%, was kept constant in all samples, whereas different tungsten contents (x) were used: 2.5, 5.0, and 7.5 wt%. The catalysts were pelletized under pressure and crushed and sieved between 0.85 and 1.25 mm. Another catalyst with a W loading of 5 wt% was prepared by simultaneous impregnation with an ammonium tungstate and nickel citrate aqueous solution. This sample was dried at 60 °C and then calcined at 550 °C for 4 h (Ni + W(5)).

2.2. Catalyst characterization

Powder X-ray diffraction (XRD) patterns were recorded on a Siemens D5000 diffractometer, equipped with a graphite monochromator and using Cu-K_α radiation.

X-ray photoelectron spectra were collected using a Physical Electronics PHI 5700 spectrometer with nonmonochromatic Mg-K_α radiation (300 W, 15 kV, 1253.6 eV) and with a multichannel detector. Spectra of powder samples were recorded in the constant pass energy mode at 29.35 eV, using a 720 μm diameter analysis area. Charge referencing was measured against adventitious carbon (C 1s 284.8 eV). A PHI ACCESS ESCA-V6.0 F software package was used to record and analyze the spectra. A Shirley-type background was subtracted from the signals. Recorded spectra were always fitted using Gauss–Lorentz curves in order to determine the binding energy of the different element core levels more accurately. The reduced samples, before the XPS analysis, were kept in *n*-hexane to avoid contact with air.

FTIR spectra were recorded by using a Thermo Optek Nexus instrument, using conventional IR cells connected to a gas manipulation apparatus. Powder samples were pressed into self-supporting disks, having an average weight of 20 mg. Before any adsorption experiment, samples were outgassed at 450 °C and cooled to room temperature.

The reducibility of the catalysts was studied by temperature-programmed reduction by hydrogen (H_2-TPR). Experiments were carried out between 40 and 700 °C, using a flow of Ar/H_2 (40 $cm^3\,min^{-1}$, 10 vol% of H_2) and a heating rate of 10 °C min^{-1}. The effluent gas was passed through a cold trap (−80 °C) before passing into the thermal conductivity detector in order to remove water from the exit stream.

The acidic properties were analyzed by temperature-programmed desorption of chemisorbed ammonia (NH_3-TPD). Before the adsorption of ammonia at 100 °C, the samples were reduced at 450 °C using a flow of H_2 (60 $cm^3\,min^{-1}$). The ammonia desorbed between 100 and 550 °C (heating rate of 10 °C min^{-1}) was analyzed by an on-line gas chromatograph (Shimadzu GC-14A) provided with a TC detector.

The specific surface areas of the solids were evaluated from the nitrogen adsorption–desorption isotherms at −196 °C in a Quantachrom Autosorb-1 apparatus, after degassing at 200 °C and 1.3×10^{-2} Pa for 24 h.

Hydrogen chemisorption was performed in a Micromeritics Asap 2010 apparatus, after the in situ reduction of sam-

ples at 450 °C (15 °C min^{-1}) for 1 h, under a flow of H_2. After reduction, the catalysts were degassed at 10^{-4} Pa for 10 h at the same temperature and cooled at 35 °C, to carry out the chemisorption of H_2. The range of pressure studied in chemisorption was 0.013–0.04 MPa and the amounts of hydrogen chemisorbed were calculated by extrapolation of the isotherms to zero pressure. Dispersion data were calculated by assuming a stoichiometry H/Ni = 1. The degree of reduction of nickel (α) was determined by oxygen chemisorption in the same apparatus. The samples were reduced and degassed under the same conditions and the oxygen chemisorption was carried out at 400 °C and the range of pressure studied was 0.013–0.08 MPa.

TEM micrographs were performed with a Phillips CM-200 high-resolution transmission electron microscope. Previously, the reduced samples were embedded in a *n*-hexane solution and suspended on a Cu grid of 3.5 mm in diameter.

2.3. Catalytic activity measurement

The hydrogenation of tetralin was performed in a high-pressure fixed-bed continuous-flow stainless-steel catalytic reactor (9.1 mm i.d. and 230 mm length) operated in the downflow mode. The reaction temperature was measured with an interior placed thermocouple in direct contact with the top part of the catalyst bed. The organic feed consisted of a solution of tetralin in *n*-heptane (5–20 vol%) and was supplied by means of a Gilson 307SC piston pump (Model 10SC). The thiotolerance of the catalysts was evaluated by adding two different concentrations of dibenzothiophene (DBT) (300 and 1000 ppm wt% for normal and severe sulfur poisoning tests, respectively) to the organic feed. A fixed volume of catalyst (3 cm^3 with particle size of 0.85–1.00 mm) without dilution was used in all cases. Prior to the activity test, the catalysts were reduced in situ at atmospheric pressure with H_2 (flow rate 60 cm^3 min^{-1}) at 450 °C for 1 h, with a heating rate of 15 °C min^{-1}. Catalytic activities were measured at different temperatures, under 6.0 MPa of hydrogen pressure, and liquid hourly space velocities (LHSV) ranging between 6.0 and 12.0 h^{-1}. The H_2/tetralin molar ratio was varied between 5.0 and 15.0. The catalytic reaction was studied by collecting liquid samples that were kept 60 min at each reaction temperature, and kept in sealed vials for posterior analysis by both gas chromatography (Shimadzu GC-14B, equipped with a flame ionization detector and a capillary column, TBR-1, coupled to an automatic injector Shimadzu AOC-20i) and mass spectrometry (Hewlett-Packard 5988A). The influence of reaction parameters such as reaction temperature, contact time, and H_2/tetralin molar ratio on the conversion and selectivity was also studied. The performance of the microreactor and the accuracy of the analytical method were studied by feeding a solution of tetralin in *n*-heptane (10 vol%) to the reactor filled with 3 cm^3 of SiC, operating at 300 °C and 6.0 MPa. No formation of foreign products was detected with a recovery percentage of the tetralin feed of 95%. In previous experiments, the variation of the amount of catalysts and the total flow rate with a constant space velocity led to no modification of conversion values. No influence of the particle diameter was found either.

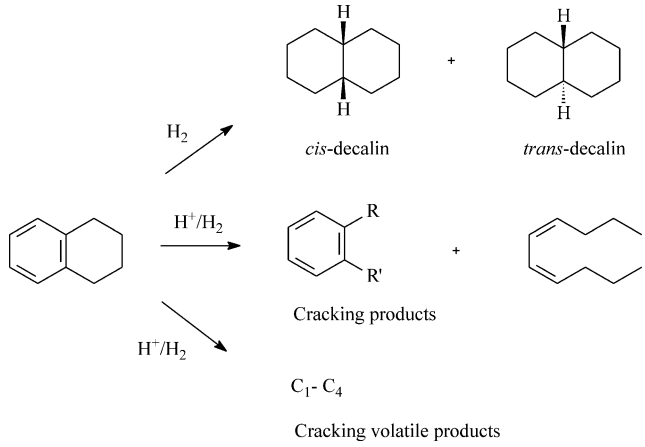

Scheme 1.

The catalysts were tested in the tetralin hydrogenation to evaluate their potential behavior in the hydrogenation of aromatic hydrocarbons in diesel fuels. A large number of products were detected by gas chromatography analysis. After identification of the majority of them, they were classified, as recently reported [12,13], into the following groups:

(i) volatile compounds (VC) that includes noncondensable C_1–C_4 products that were calculated from the carbon balance of the reaction,
(ii) hydrogenation products that include *trans*- and *cis*-decalin,
(iii) cracking compounds (CC) that include primary products such as benzene, toluene, ethylbenzene, *o*-xylene, 1-ethyl-2-methylbenzene, 1-propenyl-2-methylbenzene, *n*-propylbenzene and iso-propylbenzene, and secondary products, which are derived from ring opening reactions such as polyalkylolefins, decadiene, and cyclohexene-1-butylidene, and
(iv) naphthalene (Scheme 1).

Products heavier than decalins were not found. It must be taken into account that high yields of hydrogenation products and especially cracking compounds give rise to an increase in the cetane number of fuels. The selectivity for each product was defined as the number of moles of a reaction product/mol of converted tetralin $\times 100$.

3. Results and discussion

3.1. Influence of the preparation method

Generally, in the literature, there is no consensus about the most appropriate method for preparing supported NiW catalysts with a high metal dispersion [14]. Hence we have

Table 1
Textural and acidic properties of nickel–tungsten oxide-supported materials

Sample	Ni (wt%)	S_{BET} ($m^2\ g^{-1}$)	V_p ($cm^3\ g^{-1}$)	d_p(av) (Å)	d (nm),[a] reduced catalyst	Total acidity (μmol $NH_3\ g^{-1}$), reduced catalyst
SiZr-5	–	503	0.52	39.5	–	544
Ni + W(5)	20.3	229	0.17	34.4	10.1	736
W(5)Ni	18.8	283	0.25	35.7	8.7	772
NiW(5)	20.5	260	0.24	39.6	9.2	837
NiW(2.5)	19.3	329	0.28	33.4	8.9	756
NiW(7.5)	20.2	284	0.27	38.5	10.2	1026

[a] Calculed from XRD data according to Scherrer's equation.

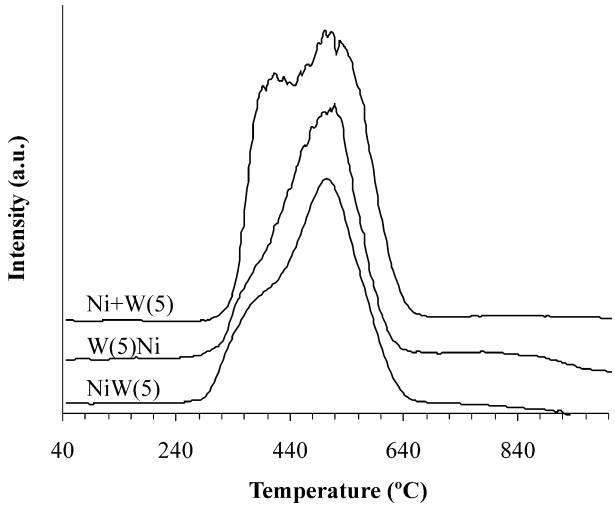

Fig. 1. H_2-TPR profiles of the unreduced samples.

carried out a preliminary study on the effect of the incorporation method of the active phase on the catalytic properties. We have prepared three materials with the same Ni:W weight ratio (20:5) but varying the impregnation method as previously described.

Textural parameters of the support and the different catalysts are listed in Table 1. All the supported NiW catalysts exhibit nitrogen adsorption–desorption isotherms of type IV in the IUPAC classification, with a shape similar to that of the support, but their specific surface areas (229–283 $m^2\ g^{-1}$) strongly decrease with respect to the support (503 $m^2\ g^{-1}$). This reduction could be due not only to the increase of the density after the incorporation of NiW by impregnation–calcination but also to a partial blockage of mesopores by large metal oxide particles.

The XRD patterns of the unreduced catalysts reveal the presence of cubic NiO crystallites, as indicated by their typical diffraction lines at 2.09 and 1.47 Å, and whose intensities increase when the support is simultaneously impregnated with the two metallic salts. However, crystalline species such as WO_3 or derived from mixed NiO–WO_3 phases were not detected. Upon reduction, the reflections at 2.03, 1.76, and 1.25 Å reveal the existence of metallic nickel. No relevant differences concerning the intensities of these peaks are found in relation to the incorporation sequence of the active phases. Metallic crystallite sizes have been estimated from the full width at half-maximum (FWHM) according to the Scherrer's equation and are also listed in Table 1.

The H_2-TPR profiles of the calcined catalysts (Fig. 1) are different from that of a supported nickel oxide catalyst obtained by using nickel citrate as an impregnation salt, whose TPR curve was composed of three peaks largely overlapping between 277 and 677 °C [8]. The supported NiW catalysts only exhibit two features centered at 377 and 500 °C. As can be observed, there are no significant differences in the position of the peaks with respect to the impregnation method. However, their relative intensities are affected, because the Ni + W(5) material shows a low temperature peak, which can be assigned to the reduction of cubic NiO species, more intense than those obtained for the catalysts synthesized by consecutive impregnation. In these latter cases, the second peak is more intense. It can be thought that if tungsten is first incorporated on the support, W(5)Ni sample, upon addition of Ni^{2+} a sublayer of $NiWO_4$ species could be formed, which would seem to avoid the formation of more reducible NiO particles in the presence of an excess of nickel. When nickel is added first, the subsequent addition of tungsten provokes the formation of a $NiWO_4$ surface which covers the dispersed NiO species, thus rendering its reduction at low temperature more difficult. The peak at 500 °C could correspond to the reduction of nickel forming part of the $NiWO_4$ phase according to the literature [15,16]. The reduction of this nickel phase takes place at lower temperatures than that observed for $NiAl_2O_4$ due to the high polarization of Ni–O bonds in $NiWO_4$ [17]. However, we have recently demonstrated that when nickel citrate is used as a nickel source, the nickel dispersed on this support also shows two peaks of H_2 consumption, the second one at 500 °C which was assigned to the presence of small NiO particles inside the mesopores and interacting strongly with the support [8]. In consequence, the second reduction peak in the TPR profile of NiW samples could be assigned to the reduction of both mixed oxide $NiWO_4$ and small NiO particles located in the mesopores. Moreover, for NiW(5) and W(5)Ni materials, the second peak has a slightly lower intensity than that observed for Ni + W(5), which means that the nickel reduction is now more difficult and, as a consequence, an important fraction of nickel remains unreduced. This fact could confer upon these catalysts a high surface acidity.

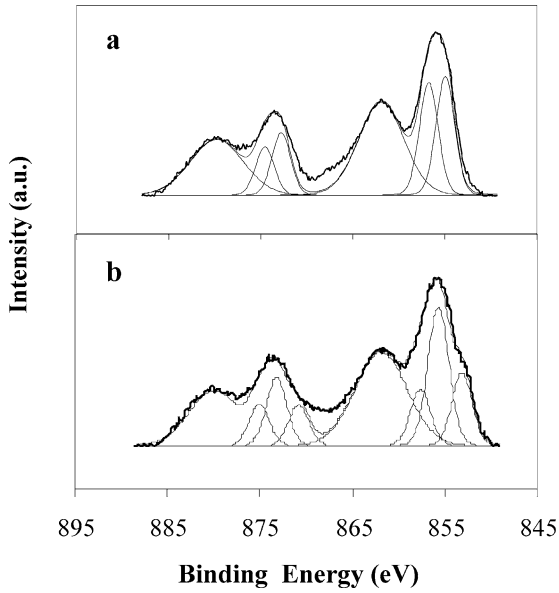

Fig. 2. Ni 2p XPS spectra of: (a) unreduced and (b) reduced NiW(5) catalysts.

In fact, the reduced NiW(5) catalyst shows the highest total acidity (837 μmol NH_3 g^{-1}), as determined by ammonia TPD between 100 and 550 °C (Table 1), probably due to the high tendency of the remaining Ni^{2+} to coordinate ammonia molecules forming amino complexes. However, this behavior contrasts with that of the Ni + W(5) catalyst, which presents the highest consumption of H_2 in the H_2-TPR curve, and shows the lowest acidity (736 μmol NH_3 g^{-1}). The H_2-TPR curves of the supported NiW catalysts do not show any peaks corresponding to the reduction of W(VI) to W(IV), which could appear at higher temperatures. Nevertheless, the XPS results (vide infra) point to a partial reduction of W(VI) to W(IV), which might be masked by the tail of the peak observed in the H_2-TPR curve at 500 °C. According to Scheffer et al. [17], tungsten ions can be reduced at lower temperatures than WO_3 by the possible effect of nickel reduction nuclei.

The presence of two different nickel phases, NiO and $NiWO_4$, on the surface of the support was confirmed by XPS. Thus, the Ni 2p core level signal of all calcined materials exhibits a single broad peak centered at ca. 856 eV and the corresponding shake-up satellite at 862 eV (Fig. 2a). The first peak can be deconvoluted in two components at 855.0 and 857.0 eV, with a similar intensity (Table 2). The first peak can be assigned to the presence of surface octahedral NiO [18], whereas the position of the second Ni $2p_{3/2}$ peak is very close to that reported in the literature for $NiWO_4$ [19,20]. However, with XPS analysis the percentage of Ni^{2+} found at 857 eV for all catalysts is very high, even higher than that expected from the tungsten content; thus, this signal must be also assigned to the presence of small particles of NiO located on the wall of the mesopores and/or to some nickel ions interacting with the $M–O^-$ groups of the support [8]. On the other hand, the binding energy for the W

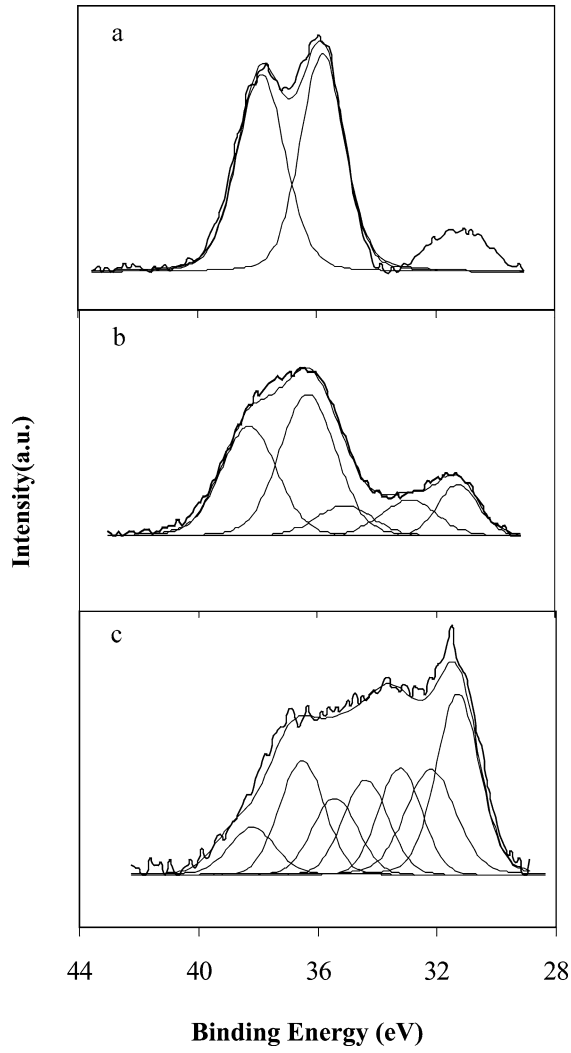

Fig. 3. W 4f XPS spectra of: (a) unreduced and (b) reduced NiW(5) catalysts and (c) spent catalyst using a feed with 300 ppm of DBT.

$4f_{7/2}$ is close to 35.5 eV (Fig. 3a), which is typical of tungsten in $NiWO_4$ [21], confirming the existence of this phase. This result confirms that tungsten is always incorporated into the catalysts forming a mixed $NiWO_4$ oxide and never as pure WO_3 oxide. The binding energies of Zr $3d_{5/2}$ and Si 2p are practically constant in all catalysts (Table 2).

After reduction, the Ni 2p core level reveals in all cases the formation of surface metallic nickel, since a new low intensity signal at 852.5–853.3 eV is observed (Fig. 2b). The percentage of Ni^0 is very low in all cases possibly as a result of the fact that photoelectrons that emerge from the core level of nickel are subsequently reabsorbed by other nickel atoms of metallic particles. However, the signals corresponding to NiO and Ni^{2+} phases at 857 eV are still present. It is noteworthy that the Ni $2p_{3/2}$ peak corresponding to NiO is now much more intense than that corresponding to Ni^{2+} at 857 eV. This high percentage of NiO can be attributed not only to the difficult detection of Ni^0 but also to a partial oxidation of the catalysts during the transport of the reduced samples from the reduction reactor to the spectrometer, be-

Table 2
XPS data for the supported NiW materials, before and after reduction

Sample	Binding energy (eV)						
	Zr $2p_{3/2}$	Si 2p	O 1s	Ni $2p_{3/2}$		W $4f_{7/2}$	
				Ni^{2+}	Ni^0	W^{6+}	W^{4+}
SiZr-5	182.8	102.8	532.8	–	–	–	–
Unreduced catalysts							
Ni + W(5)	182.7	103.2	532.6	855.3 857.2	–	35.5	–
W(5)Ni	182.9	103.4	532.9	855.0 856.7	–	35.6	–
NiW(5)	182.5	102.9	532.8	855.2 856.9	–	35.8	–
NiW(2.5)	182.9	103.2	532.9	854.9 856.9	–	35.6	–
NiW(7.5)	182.7	103.4	532.8	854.9 856.8	–	35.5	–
Reduced catalysts							
Ni + W(5)	182.8	103.0	532.4	855.3 857.2	852.6	35.8 (84%)	32.9 (16%)
W(5)Ni	182.9	103.0	532.4	855.2 857.2	852.5	35.8 (88%)	32.9 (12%)
NiW(5)	182.7	103.3	532.5	855.7 857.6	853.3	36.3 (65%)	32.9 (35%)
NiW(2.5)	182.7	103.0	532.4	855.4 857.4	852.8	35.8 (41%)	32.9 (59%)
NiW(7.5)	182.8	103.0	532.5	855.2 857.2	852.4	36.1 (50%)	32.9 (50%)

cause nickel forming part of small particles of NiO inside the pores or as $NiWO^4$ is more difficult to reduce, as deduced from the H_2-TPR curves. As regards the W $4f_{7/2}$ core level signal (Fig. 3b), it is also modified after reduction due the appearance of a peak at 32.9 eV assigned to W(IV) [22]. However, a photoelectron Zr 4p signal is also observed at 30 eV. Interestingly, the supported NiW(5) catalyst shows the maximum tungsten reduction, demonstrating that the addition of tungsten over nickel favors the reduction of the surface mixed $NiWO_4$ oxide. The presence of W(IV) ions could also contribute to the high acidity of this catalyst. In contrast, the W(5)Ni catalyst shows the lowest percentage of tungsten reduction, possibly due to the difficulty of reduction of $NiWO_4$ located under the NiO layer.

The metallic properties of reduced catalysts are compiled in Table 3. In general, the reduction degree (α), obtained from oxygen chemisorption at 400 °C, is in good agreement with the results found by H_2-TPR. Thus, the more easily reducible catalyst is Ni + W(5), with a reduction degree of 88.7%. In contrast, W(5)Ni is the catalyst which shows the lowest degree of reduction, but this material presents the highest metallic dispersion and metallic surface area, possibly because the formation of $NiWO_4$ inhibits the agglomeration of NiO particles. In fact, the average metal particle size for this catalyst is very small (Table 3). The micrographs of the reduced NiW(5) and W(5)Ni catalysts (Fig. 4) display metallic particles within a broad range of sizes, the average particle sizes being smaller for the W(5)Ni sample, according to H_2 chemisorption. The particle sizes obtained by the different measurement methods are not coincident; however, the relative order of the metallic particle sizes corresponding to the studied catalysts is maintained.

Table 3
Metallic characteristics for the reduced nickel–tungsten supported catalysts

Catalysts	α (%)	D (%)	S_{met}		d (nm)	
			(m^2/g_{cat})	(m^2/g_{Ni^0})	H_2	TEM
Ni + W(5)	88.7	3.5	5.2	23.0	23.6	8.8
W(5)Ni	30.9	11.0	13.9	73.1	7.4	1.5
NiW(5)	61.7	6.2	8.4	41.0	13.3	7.0
NiW(2.5)	74.7	3.7	4.5	24.8	21.9	8.6
NiW(7.5)	57.1	5.4	6.8	35.7	15.2	7.8

α is the reduction degree determined by chemisorption of O_2, D the metallic dispersion, and d the average diameter of the metallic crystallite.

The study of the surface properties of this family of catalysts has been completed by adsorption of CO coupled to IR spectroscopy. The spectra of surface species arising from CO adsorption over reduced catalysts are shown in Fig. 5. In the region 2000–2100 cm^{-1}, a main CO band appears split at about 2050 and 2080 cm^{-1}, the first component being more intense. According to the literature, both bands can be assigned to CO linearly adsorbed over reduced metal centers [23,24], but with different strengths. In particular, the component at lower frequencies has been found after CO adsorption on Ni(100), Ni(110), and Ni(111) planes of large particles. The intensity of the band at 2050 cm^{-1} decreases

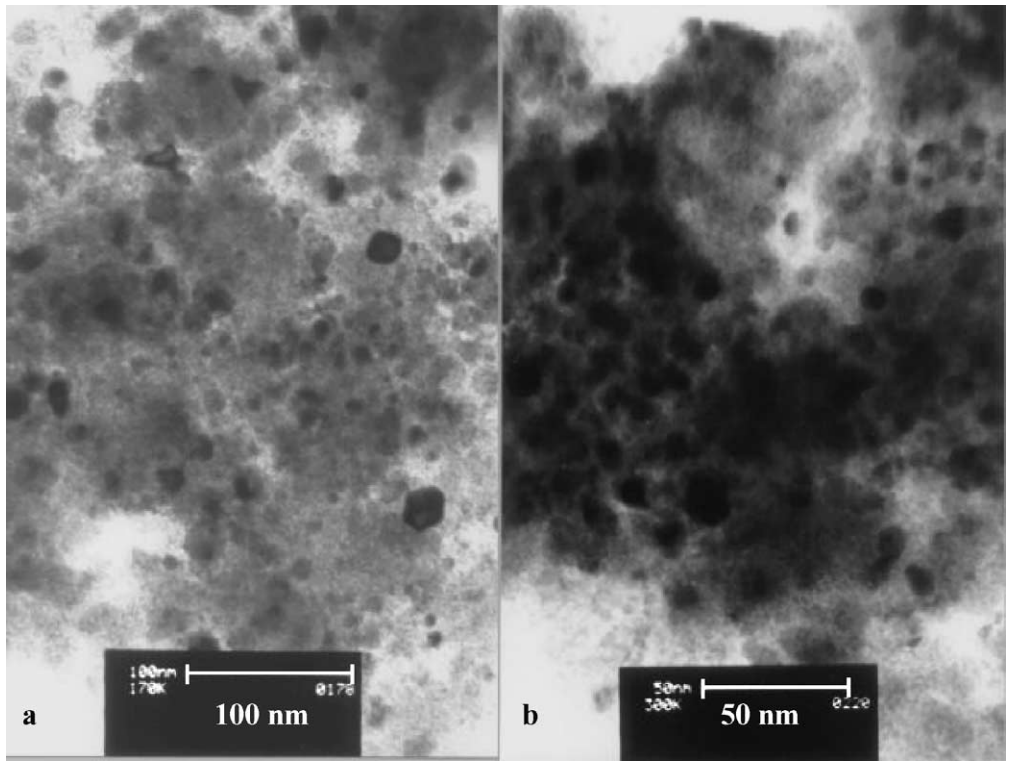

Fig. 4. Transmission electron micrographs of: (a) W(5)Ni and (b) NiW(5) catalysts.

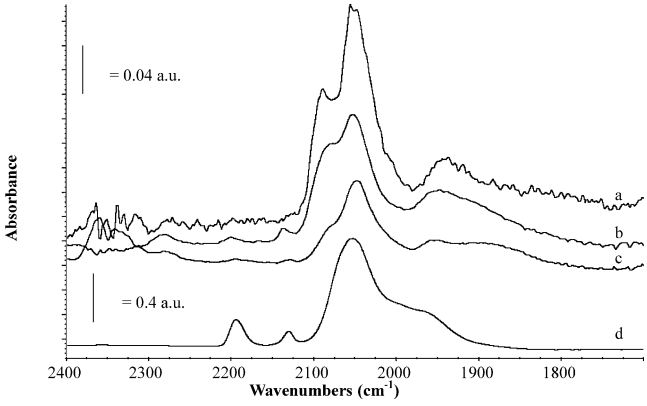

Fig. 5. FTIR spectra of surface species arising from CO adsorption over: (a) reduced Ni + W(5), (b) reduced NiW(5), (c) reduced W(5)Ni, and (d) a fresh NiW(5) sample, in the presence of 1 Torr of CO.

slowly in the order Ni + W(5) > NiW(5) > W(5)Ni, which is in good agreement with the decrease in the degree of reduction of these catalysts (Table 3).

On the other hand, the higher frequency of the stretching band (2080 cm^{-1}) is attributed to CO linearly bonded to small particles, which implies a weaker metal–CO interaction due to either some property of these small particles or a strong metal–support interaction [25]. In fact, a band around 2090 cm^{-1} has also been more precisely assigned to CO coordinated to isolated Ni^0 adjacent to oxygen atoms of an alumina support [6]. The component at higher frequencies is more evident in the Ni + W(5) sample and it is centered at 2090 cm^{-1}, becoming less defined in the NiW(5) sample (2076 cm^{-1}) and no more than a weak shoulder at 2073 cm^{-1} in the W(5)Ni catalyst. Taking into account its attribution to weakly adsorbed Ni^0–CO species, this would indicate that the Ni + W(5) sample is more reduced than the other two catalysts. This result completely agrees with the reduction degrees determined by oxygen chemisorption. The small shift of the position of the maximum could be due to an increasing electron withdrawal effect owing to the decrease of the metal particle size in these catalysts.

After prolonged outgassing at room temperature, the spectra are significantly changed (Fig. 6). The intensities are consistently lowered and those bands due to CO coordinated over metallic centers shifted toward lower wavenumbers, around 2050 cm^{-1}, as was expected for lower CO coverage. The two components discussed above are not already evident and spectra only show a broad and complex band due to CO strongly adsorbed over reduced centers. The spectrum of W(5)Ni exhibits now a sharper band centered at 2040 cm^{-1}, thus, it seems likely that this sample has a more homogeneous metallic distribution, as expected from the low average metal particle size in this catalyst (Table 3).

The spectrum recorded following CO adsorption (1 Torr) over a fresh NiW(5) catalyst (Fig. 5) shows a band around 2050 cm^{-1}. The appearance of this band, assigned to the Ni^0–CO interaction, could indicate that the surface of this sample has been reduced under an atmosphere of CO. Alternatively, this band could be assigned to the asymmetric stretching of $Ni^+(CO)_2$ [26]. A band at 2200 cm^{-1} also appears in the spectrum of the fresh catalyst treated with

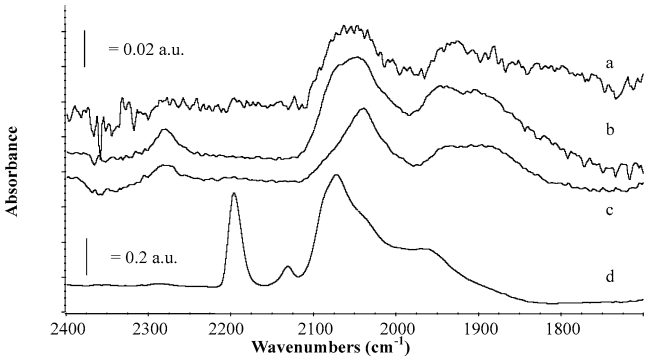

Fig. 6. FTIR spectra of adsorbed species arising from CO adsorption, after outgassing at room temperature, over: (a) reduced Ni + W(5), (b) reduced NiW(5), (c) reduced W(5)Ni, and (d) fresh NiW(5) samples.

CO which could be assigned to Ni^{2+}–CO species [26]. In fact, in the case of nickel ions in the ZSM-5 matrix, Hadjiivanov et al. [26] pointed out the existence of a predominant δ-bond character in this interaction, thus explaining the high frequency of the carbonyl species (2200 cm^{-1}) and its high stability with outgassing at room temperature. The same authors observed two bands at 2136 and 2092 cm^{-1} assigned to symmetric and asymmetric stretching in $Ni^{+}(CO)_2$ species. In our case, a band is also visible at 2130 cm^{-1}, which could be assigned to the presence of such $Ni^{+}(CO)_2$ species. Primet et al. [27] also observed two bands at 2070–2080 cm^{-1} corresponding to CO coordinated over Ni^{2+} ions interacting with an oxide phase. The weak bands at 2200 and 2130 cm^{-1} have also been detected in the spectra of CO adsorbed over reduced samples, indicating that CO is coordinated over residual Ni^{2+}/Ni^{+} species. The relative intensities are, however, inverted with respect to the same bands in the fresh sample, so it is evident that the species characterized by the band at 2200 cm^{-1} are more easily reduced. These weak bands disappeared after outgassing the reduced catalysts at room temperature (Fig. 6). The presence of Ni^{2+} species interacting with CO was expected due to the low degree of reduction attained in these catalysts under the experimental conditions chosen in the present work.

Finally, in the region of the spectrum below 2000 cm^{-1}, it is possible to detect a quite complex band in the spectra of the three reduced catalysts with a maximum at 1945 cm^{-1}, and another one in the spectrum of W(5)Ni at 1900 cm^{-1}. These bands are assigned to bridged and threefold bridged CO over metal centers [28]. The appearance of this small absorption band at 1900 cm^{-1} in the W(5)Ni reduced catalyst could be due to the decrease in cluster size. This is in good agreement with the results obtained from other techniques which point out that this is the catalyst with the lowest diameter of metallic crystallites and the highest metal dispersion.

Once the supported NiW catalysts had been characterized, their catalytic behavior in the hydrogenation and ring opening of tetralin was evaluated. Total tetralin conversion and yield to the different reaction products, as a function of the reaction temperature, for the three catalysts above described, are shown in Fig. 7. At low reaction temperatures

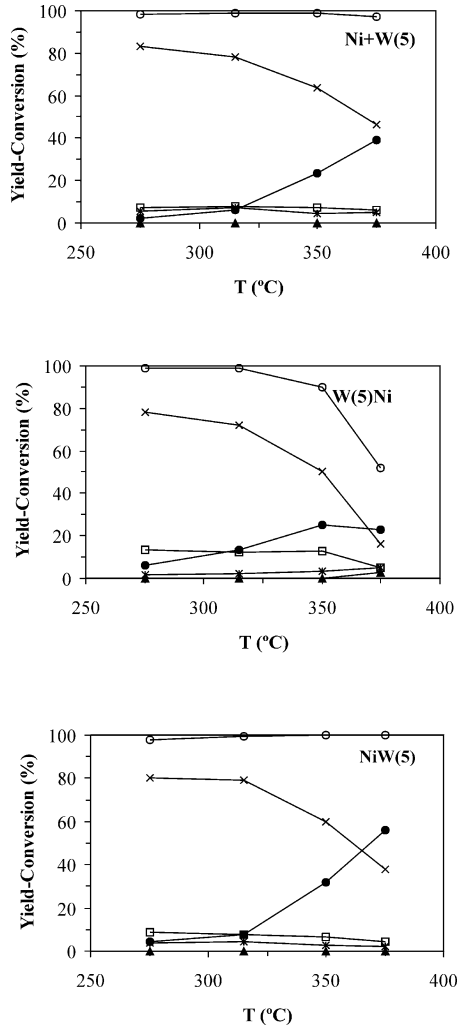

Fig. 7. Yield and conversion for tetralin hydrogenation as a function of the reaction temperature: (○) conversion, (×) *trans*-decalin, (□) *cis*-decalin, (●) CC, (▲) naphthalene, and (∗) VC. Experimental conditions: H_2/THN molar ratio = 10.1; $P(H_2)$ = 6 MPa; contact time = 3.6 s.

(275 and 315 °C), the conversion was in all cases higher than 97%. However, at higher temperatures, the conversion for the W(5)Ni catalyst fell to 89.9% at 350 °C and 52.1% at 375 °C, whereas the other two catalysts maintained their conversion close to 100%. With regard to the yields of the different reaction products, it is noteworthy that, in all cases, the formation of naphthalene and volatile compounds (VC) was negligible even at high reaction temperatures. It is also found that the production of *trans*-decalin, which is the main reaction product at low temperatures (ca. 80%), decreases by increasing the reaction temperature. This behavior is to be expected if we take into account the exothermic character of the hydrogenation of tetralin, which is favored at low temperatures [29,30]. However, in accordance with the endothermic character of C–C bond cleavage, the NiW(5) and Ni + W(5) catalysts showed an important increase of the CC yield with the reaction temperature, reaching the values of 56.1 and 39.3%, respectively at 375 °C. The W(5)Ni catalyst was the least selective toward CC, with a maximum

yield at 350 °C of 25.0%. This could be attributed to the fact that the formation of metallic nickel particles on the $NiWO_4$ sublayer on the support surface impedes the access of tetralin molecules to Ni^{2+} and W(VI)/W(IV) acid centers. It must be noted that although the hydrogenation of aromatics is generally recognized to be a metal-catalyzed reaction, many authors [31–36] have reported that, in addition to metal centers, the acid sites of the support also play an important role in the hydrogenation step. This phenomenon seems to be attributed to the hydrogen spilled over from the metal surface which gives rise to the hydrogenation of aromatic molecules adsorbed on acid sites. The inaccessibility to this $NiWO_4$ sublayer is the cause of the lowest degree of reduction of W(VI) observed for this catalyst. These catalytic results match well with the surface properties of these catalysts. Thus, W(5)Ni, having the highest dispersion and the lowest metallic particle size, shows a better performance in tetralin hydrogenation at low temperatures, although its conversion quickly decreases as the reaction temperature is raised. NiW(5) exhibits the greatest capacity to form CC compounds due to its high acidity and the more external location of such acid centers, Ni^{2+} and W(VI)/W(IV). Interestingly, this NiW(5) catalyst maintains a good level of activity, at moderate temperatures, toward hydrogenation products (42.7%). This catalyst has a better conversion and a much better yield of CC than a nickel-based catalyst prepared by using the same support and with a similar loading [8]. Moreover, NiW(5) exhibits a similar performance in the hydrogenation of tetralin compared to NiMo catalysts supported on alumina pillared α-zirconium phosphate with a composition of 20 wt% of nickel and 5–10 wt% of molybdenum [13]. Thus, the catalyst obtained by consecutive impregnations, first with Ni and then with W, appears to be more effective in the reactions of hydrogenation and ring opening of tetralin. Therefore, it can be concluded that the preparation method appears to be a key factor in determining the properties of a catalyst and, as a consequence, the activity and selectivity in the catalytic reaction, as previously described for CoMo and NiW sulfide catalysts [37–39]. Likewise, Bendezú et al. [39] have also concluded that the preparation method has a strong influence on the dispersion and location of Ni and W sulfides supported on USY zeolite, determining the initial HDS activity of the catalysts.

3.2. Study of the reaction conditions

The NiW(5) catalyst, which showed the best catalytic properties of the series, was selected to study the influence of the H_2/tetralin molar ratio and contact time on the catalytic performance at 375 °C. Fig. 8a shows the variation of the conversion and the yield as a function of the molar ratio, but with the contact time maintained at 3.6 s. It can be observed that the increase of this ratio gives rise to an important increment in the tetralin conversion, the maximum value being achieved for a H_2/tetralin molar ratio of 10. This is especially due to the important enhancement of hydrocracking

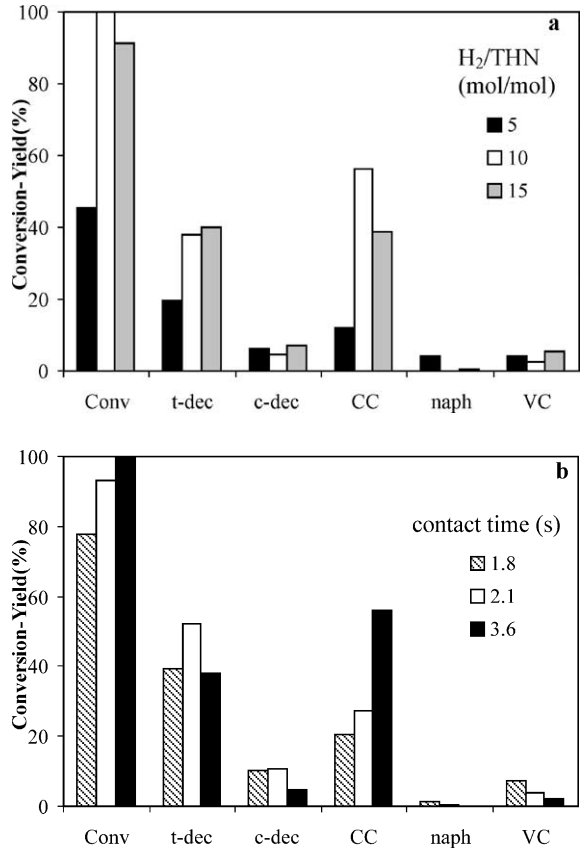

Fig. 8. Evolution of the conversion and the yield of the different reaction products on the NiW(5) catalyst at 350 °C as a function of (a) H_2/THN molar ratio (contact time 3.6 s) and (b) contact time (H_2/THN = 10.1).

reactions leading to the formation of CC products (56.1%) under these experimental conditions.

On the other hand, the influence of the contact time was also evaluated by varying this parameter between 1.8 and 3.6 s and maintaining the H_2/tetralin molar ratio constant at 10 (Fig. 8b). With a long contact time, i.e., 3.6 s, the maximum value of conversion (ca. 100%) is achieved, due mainly to the enhancement of the ring-opening reaction with CC formation.

3.3. Thiotolerance study

It is well known that nickel catalysts are easily poisoned by sulfur-containing compounds. We have studied the effect of the addition of 300 and 1000 ppm of DBT to the organic feed on the catalytic behavior of the NiW(5) catalyst.

Fig. 9 shows the conversion of tetralin as a function of time on stream at 375 °C. In the presence of 300 ppm of DBT, tetralin conversion slightly decreases in comparison with the catalytic behavior in the absence of DBT and remains close to 80% with time on stream. This can be explained by the decrease in CC formation, since the hydrogenation reaction, i.e., the formation of *cis*- and *trans*-decalin, is even favored. This means that tungsten ions are modified by the presence of sulfur, possibly forming a

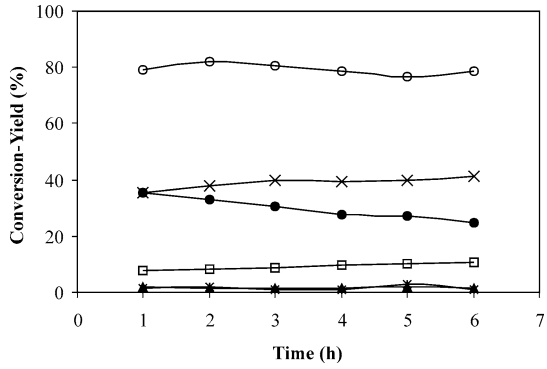

Fig. 9. Variation of conversion and yield of the different reaction products versus the time on stream for the NiW(5) catalyst in the presence of 300 ppm of DBT: (○) conversion, (×) *trans*-decalin, (□) *cis*-decalin, (●) CC, (▲) naphthalene, and (∗) VC. Reaction conditions: $T = 375\,^{\circ}\mathrm{C}$, $H_2/\mathrm{THN} = 10.1$, contact time = 3.6 s.

tungsten sulfide which displays hydrogenation properties, thus diminishing its acid properties and, as a consequence, slightly decreasing the ring opening reaction. This fact has been confirmed by XPS of the spent catalyst, which exhibits a doublet peak of $W4f_{7/2}$ and $W4f_{5/2}$ at 32.2 and 34.4 eV, respectively, corresponding to WS_2 (Fig. 3c). This catalyst, after 6 h of time on stream, still shows a yield of 25% of CC and 52% of hydrogenation products. However, if this catalyst, after 6 h of time on stream, is again treated with a feed free of sulfur, the conversion decays from 78.4 to 66.4%, with a slight decrease in the production of both CC and hydrogenation compounds. Interestingly, when the catalyst is regenerated under a flow of H_2 at 450 °C it almost recovers its initial conversion (89.5%), maintaining the yield of CC (25.0%) and increasing the yield of hydrogenation compounds (62.8%). However, when the regenerated catalyst is treated with a feed containing 1000 ppm of DBT, the conversion fell to 58.6%. The incorporation of a high concentration of DBT to the feed provokes the poisoning of nickel particles; thus, the catalyst loses not only the hydrocracking properties but also its hydrogenation activity in part. This was confirmed by the chemical analysis of a spent catalyst which had a sulfur content of 2 wt%. Nevertheless this catalyst, after 6 h on stream, presents a conversion of 58.6% and with a 42.4% of hydrogenation products and 12.8% of CC. However, the regeneration of this catalyst by treating with H_2 was not effective.

3.4. Influence of the W loading

Finally, two other catalysts with a 2.5 and 7.5 wt% of tungsten and 20 wt% of nickel loading have also been prepared by consecutive impregnation, similarly to the NiW(5) catalyst, and tested in the hydrogenation and ring opening of tetralin. The catalytic behavior of NiW(2.5) is quite similar to that of NiW(5), with a conversion at the maximum temperature (375 °C) of 96.5% and a good yield of CC formation (51.9%) and hydrogenation products (43.5%). By comparing these results with those of the NiW(5) catalyst, the hydrogenation capacity of NiW(2.5) is seen to be almost the same but the yield of CC is slightly lower in accordance with its acidity (Table 1). In contrast, the NiW(7.5) catalyst shows quite different catalytic properties with the conversion drastically falling at temperatures higher than 315 °C, the hydrogenation and ring-opening activities being very weak, specially at 375 °C. The low formation of CC compounds with this catalyst is noteworthy despite being the most acidic, since it exhibits a low degree of nickel reduction (Table 3) and it would seem that the adsorbed molecules on the acid centers do not receive enough hydrogen from the metallic centers for hydrogenation and ring opening reactions.

4. Conclusions

Nickel–tungsten impregnated mesoporous silica with a Ni loading of 20 wt% and a W loading of 5 wt% is an excellent catalyst for the hydrogenation and ring opening of tetralin subjected to high hydrogen pressure, with a good thiotolerance. The impregnation order also affects the dispersion and the nature of the active phases and, as a consequence, the performance of the catalysts. The consecutive impregnation of nickel and tungsten seems to be the best procedure for obtaining a catalyst with an improved ring opening activity and thiotolerance.

Acknowledgments

Financial support for this research was obtained under Project MAT2000-1144 (CICYT, Spain), for which we are very grateful. D.E.Q. also thanks the Ministry of Science and Technology for a fellowship.

References

[1] H. Yasuda, Y. Yoshima, Catal. Lett. 46 (1997) 43.
[2] B.H. Cooper, B.B.L. Donnis, Appl. Catal. A 137 (1996) 203.
[3] T. Halachev, P. Atanasova, A.L. Agudo, M.G. Arias, J. Ramírez, Appl. Catal. A 136 (1996) 161.
[4] J. Ramírez, P. Castillo, L. Cedeno, R. Cuevas, M. Castillo, J.M. Palacios, A.L. Agudo, Appl. Catal. A 132 (1995) 317.
[5] J. Ramírez, L. Ruiz-Ramírez, L. Cedeno, V. Harle, M. Vrinat, M. Breysse, Appl. Catal. A 93 (1993) 163.
[6] T. Halachev, R. Nava, L. Dimitrov, Appl. Catal. A 169 (1998) 111.
[7] A. Corma, A. Martinez, V. Martinez Soria, J.B. Monton, J. Catal. 153 (1995) 25.
[8] D. Eliche Quesada, J. Mérida Robles, P. Maireles Torres, E. Rodríguez Castellón, A. Jiménez López, Langmuir 19 (2003) 4985.
[9] K. Ito, Y. Kogasaka, H. Kurokawa, M. Ohshima, K. Sugiyama, H. Miura, Fuel Process. Technol. 79 (2002) 77.
[10] J.R. Chang, S.L. Chang, J. Catal. 176 (1998) 42.
[11] A. Jiménez López, E. Rodríguez Castellón, P. Maireles Torres, L. Díaz, J. Mérida Robles, Appl. Catal. A 218 (2001) 295.
[12] E. Rodríguez Castellón, L. Díaz, P. Braos García, J. Mérida Robles, P. Maireles Torres, A. Jiménez López, A. Vaccari, Appl. Catal. A 240 (2003) 83.

[13] R. Hernández Huesca, J. Mérida Robles, P. Maireles Torres, E. Rodríguez Castellón, A. Jiménez López, J. Catal. 203 (2001) 122.
[14] P. Atanasova, T. Halachev, Appl. Catal. A 108 (1994) 123.
[15] K. Choong-Hyon, L.I. Wang, L. In Chul, I.W. Seong, Appl. Catal. A 144 (1996) 159.
[16] J. Ramírez, A. Gutiérrez Alejandre, Catal. Today 43 (1998) 123.
[17] B. Scheffer, P. Molhoek, J.A. Moulijn, Appl. Catal. A 46 (1989) 11.
[18] J.C. Klein, D.M. Hercules, J. Catal. 82 (1983) 424.
[19] L. Salvati, L.E. Makovsky, J.M. Stencel, F.R. Brown, D.M. Hercules, J. Phys. Chem. 855 (1981) 3700.
[20] S.S. Chan, I.E. Wachs, L.L. Murrell, N.C. Dispenziere Jr., J. Catal. 92 (1985) 1.
[21] K.T. Nog, D.M. Hercules, J. Phys. Chem. 80 (1976) 2094.
[22] J.F. Moulder, W.F. Stickle, P.E. Sobol, K.D. Bomben, in: J. Chastain (Ed.), Handbook of X-Ray Photoelectron Spectroscopy, Perkin-Elmer, Minneapolis, 1992.
[23] K. Hadjiivanov, M. Mihaylov, N. Abadijeva, D. Klissurski, J. Chem. Soc., Faraday Trans. 94 (1998) 3711.
[24] J. Fierro (Ed.), Spectroscopic Characterization of Heterogeneous Catalysts, in: Stud. Surf. Sci. Catal., Vol. 57, Elsevier, New York, 1990.
[25] K. Coulter, X. Xu, D.W. Goodman, J. Phys. Chem. 98 (1994) 1245.
[26] K. Hadjiivanov, H. Knotzinger, M. Mihaylov, J. Phys. Chem. B 106 (2002) 2618.
[27] M. Primet, J.A. Dalmon, G.A. Martin, J. Catal. 46 (1977) 25.
[28] K.I. Hadjiivanov, G.N. Vayssilov, Adv. Catal. 47 (2002) 308.
[29] T. Fujikawa, K. Idei, T. Ebihara, H. Mizuguchi, K. Usui, Appl. Catal. A 192 (2000) 253.
[30] A. Corma, A. Martínez, V. Martínez Soria, J. Catal. 169 (1997) 480.
[31] K.C. Park, D.J. Yim, S.K. Ihm, Catal. Today 74 (2002) 281.
[32] M.A. Arribas, A. Martínez, Appl. Catal. A 230 (2002) 203.
[33] P. Chou, M.A. Vannice, J. Catal. 107 (1987) 129.
[34] M.V. Rahaman, M.A. Vannice, J. Catal. 127 (1991) 251.
[35] S.D. Lin, M.A. Vannice, J. Catal. 143 (1993) 539.
[36] J. Wang, Q. Li, J. Yao, Appl. Catal. A 184 (1999) 181.
[37] A.M. Venezia, V. La Parola, G. Deganello, D. Cauzzi, G. Leonardi, G. Predieri, Appl. Catal. A 229 (2002) 261.
[38] P. Atanasova, T. Tabakova, C. Vladov, T. Halachev, A. López Agudo, Appl. Catal. A 161 (1997) 105.
[39] S. Bendezú, R. Cid, J.L.G. Fierro, A. López Agudo, Appl. Catal. A 197 (2000) 47.